



CHORUS

This is the accepted manuscript made available via CHORUS. The article has been published as:

Coulomb-Driven Energy Boost of Heavy Ions for Laser-Plasma Acceleration

J. Braenzel, A. A. Andreev, K. Platonov, M. Klingsporn, L. Ehrentraut, W. Sandner, and M. Schnürer

Phys. Rev. Lett. **114**, 124801 — Published 26 March 2015

DOI: [10.1103/PhysRevLett.114.124801](https://doi.org/10.1103/PhysRevLett.114.124801)

Coulomb driven energy boost of heavy ions for laser plasma acceleration

J. Braenzel,^{1,2} A. A. Andreev,^{1,3,4} K. Platonov,³ M. Klingsporn,⁵ L. Ehrentraut,¹ W. Sandner,^{1,2,6} and M. Schnürer¹

¹Max Born Institute, Max Born Str. 2A, 12489 Berlin, Germany

²Technical University Berlin, Strasse des 17. Juni 135, 10623 Berlin, Germany

³Vavilov State Optical Institute, Birzhevaya line 12, 199064 St. Petersburg, Russia

⁴St. Petersburg University, University emb.6, St. Petersburg 199064, Russia

⁵IHP, Im Technologiepark 25, 15236 Frankfurt

⁶ELI-DC International Association AISBL

(Dated: March 9, 2015)

An unprecedented increase of kinetic energy of laser accelerated heavy ions is demonstrated. Ultra thin gold foils have been irradiated by an ultra short laser pulse at a peak intensity of 8×10^{19} W/cm². Highly charged gold ions with kinetic energies up to > 200 MeV and a bandwidth limited energy distribution have been reached by using 1.3 Joule laser energy on target. 1D and 2D Particle in Cell simulations show how a spatial dependence on the ions ionization leads to an enhancement of the accelerating electrical field. Our theoretical model considers a spatial distribution of the ionization inside the thin target leading to a field enhancement for the heavy ions by Coulomb explosion. It is capable of explaining the energy boost of highly charged ions, enabling a higher efficiency for the laser driven heavy ion acceleration.

PACS numbers:

Laser driven ion acceleration has gained a wide scientific interest, as it is a promising ion source for investigation in basic plasma physics and for application in accelerator technology [1, 2] related to bio-medical [3, 4] and hadron research [5]. While the acceleration of protons and light ions are intensively investigated during the last decade, little is reported on acceleration of heavier ions [6]. Such knowledge is mandatory to achieve the objectives of upcoming new laser facilities [7, 8], e.g. the exploration of nuclear, astrophysical questions as well as the potential use as beam lines for heavy ion radio therapy [9]. Energies of heavy ions exceeding the mass number $A \gg 12$ with $E_{kin}/u \sim 1 - 2$ MeV/u (energy per nucleon) have been reported so far [6, 10], by using short pulse laser systems with laser pulse energies well above 20 J [11].

In the following we report and discuss a considerable energy boost for acceleration of highly charged heavy ions with only using 1.3 J on an ultra thin heavy material target. We accelerated ions up to $E_{Max}/u > 1$ MeV/u, with a bandwidth limited energy distribution. We found a remarkable deviation in the maximum energy to charge Z scaling in comparison to established models of Mora [12] and Schreiber [13, 14].

Presently used laser ion acceleration schemes like Target Normal Sheath Acceleration (TNSA) [15], or leaky light sail / Radiation Pressure Acceleration (RPA) [16–18], Coherent Acceleration of Ions by Laser (CAIL) [4, 19], Break Out Afterburner (BOA) [20] make use of an energy transfer from laser to electrons and in a following step from electrons to ions. In the typical physical picture an ultra intense laser pulse is focused on a thin target, ionizes it and displaces the electrons from the ion background. This creates a high electrical field at the rear and front side of the target. The Coulomb attrac-

tion field of the ions circumvents the electrons escape and enables the acceleration of the ions. For ultra thin targets and relativistic laser intensities the acceleration is enhanced by the transparency of the target and the relativistic kinematics of the electrons [18, 21–23]. Further optimization for the energies of light ions is proposed by a Coulomb exploding background of heavy ion constituents in a ultra thin foil target [24–26]. A remarkable contribution by the Coulomb explosion to the energy of very heavy ions energy is predicted but still under theoretical discussion [27, 28].

Most acceleration models assume an averaged degree of ionization leading to a fixed electron density - which creates the moving accelerating electrical field for the ions. During the laser plasma interaction ions of different charge to mass ratio Z/A separate in the velocity picture, leading to higher MeV/u for the lighter material. The energy per nucleon decreases significantly with the decreasing charge to mass ratio, as the accelerating field is screened by the light ions. Laser plasma experiments using thin foils showed, that in the presence of hydrogen and carbon, ions with a smaller Z/A ratio are not accelerated at all or stay with much lower velocity [10]. Only specially prepared, heated targets without contamination by light ions, enabled an acceleration of the heavy ions up to the MeV/u range. To our knowledge we obtained for the first time heavy ions with > 1 MeV/u in presence of the contamination layer. While the maximum kinetic energy E_{kin}^{Max} for hydrogen reach 12 MeV/u and 4.2 MeV/u for C^{6+}/O^{8+} , the highest charged gold ion $\gtrsim Au^{50+}$ follows with $\gtrsim 1$ MeV/u. Experiments have been performed at the Max Born Institute High Field Ti:Sapph. laser. It delivers 1.3 J at (30 – 35) fs on the target after contrast enhancement by a XPW [29] front-end and a Double Plasma Mirror (DPM) [30], leading

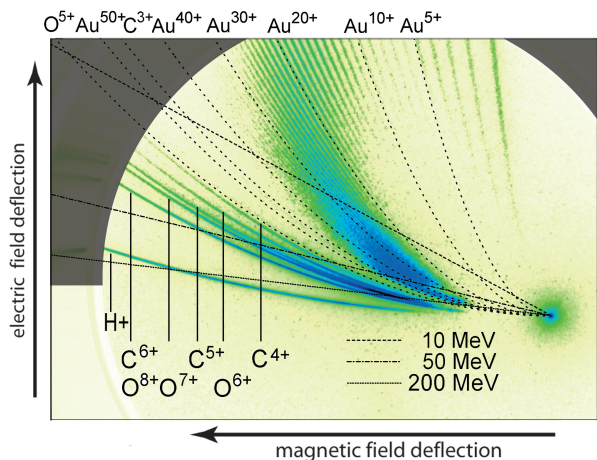


FIG. 1: Raw spectra from Thomson spectrometer (single shot measurement), particle density in false color coding. Each trace represents a different charge to mass ratio Z/m . Gray shade indicates end of detector. Light ion traces (H^+ , C^{6+} - C^{3+} , O^{8+} - O^{5+}) are identified. Overlay shows theoretical parabolas at different charge states of gold ions (black dots). Straight lines mark theoretical constant energy at each degree of ionization for gold, $m = 197$ u.

to a pre pulse free peak to ASE contrast of $\leq 10^{-14}$ in the minor ps range. The laser is focused by a $f/2.5$ off axis parabola to a focal FWHM size of $\sim 4 \mu\text{m}$, giving an peak intensity of $8 \times 10^{19} \text{ W/cm}^2$. The normalized laser field is $a_0 = qE_L/m_e c \omega = 6$ for linear polarization, with the electron mass m_e and charge q , laser frequency ω and speed of light c , respectively. We focused the laser at free standing $(14 \pm 2) \text{ nm}$ gold foil [31], which we produced by thermal evaporation at 10^{-6} mbar (deposition rate: 0.2 nm/s), followed by a floating process. HRTEM (High Resolution Transmission Electron Microscopy) reveals a polycrystalline structure of the gold formed by an island growth mode on a carbon based supportive film, which we identify as the rest of the parting agent. The average grain size is of the order of 10 nm . Determination of the composition has been carried out by EDX (Energy Dispersive X-Ray Spectroscopy) with a state of the art FEI ChemiSTEMTM system and was quantified standardless with a Cliff-Lorimer calculation. The foil consists of gold 96%, carbon 2–3% and oxygen 2%, hydrogen is not determined. STEM (Scanning Transmission Electron Microscopy) measurements reveals a sub crack like structure in $(10-20) \text{ nm}$ distance (see Fig.3b). Structured surfaces can increase the absorption of the laser light, leading to a higher efficiency of the acceleration mechanism. This is at the moment discussed widely, but yet has not been considered for the thinnest targets [32, 33]. Accelerated particles were detected in single shot measurement by a Thomson spectrometer at 0° in laser propagation direction. The setup consists of an entering pinhole with a diameter of $110 \mu\text{m}$, a permanent magnet, electrical field

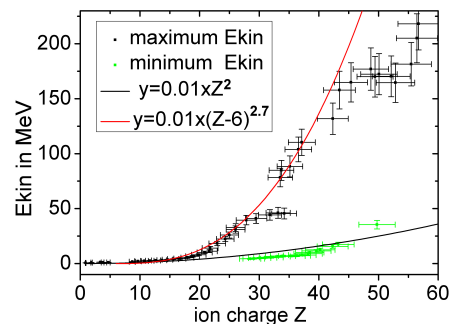


FIG. 2: Maximum (black) and minimum (green) kinetic energy of gold ions in dependence of their charge state Z . For $Z < 25$ the detectors range is cutting the low energetic part of the spectra. Red line shows a $(Z-6)^{2.7}$ and black line a Z^2 to E_{kin}^{Max} , both fit functions with the same scaling coefficient.

plates and a 100 mm Multi Channel Plate (MCP Hamamatsu) covering a detection angle of $1 \times 10^{-7} \text{ sr}$ from the target [34]. Measurements at a lower laser contrast (without DPM) $\leq 10^{-11}$, showed much lower E_{kin}^{Max} and particle numbers for hydrogen, carbon, oxygen ions and no gold ion spectra in the measured energy range.

Fig.1 shows a captured picture of the detector. We identify traces of accelerated gold particles for ionization degrees reaching from Au^{1+} to $> Au^{50+}$, well beyond the C^{3+} trace. With increasing charge to mass ratio we observe light ions traces of oxygen, carbon and hydrogen. For a quick interpretation of the measured data, the overlay in Fig.1 shows lines of constant energy for $m = 197 \text{ u}$ to mark constant energy positions for different charge states on the detector. We observed a strong signal for gold ions between Au^{20+} and the highest degree of ionization $> Au^{50+}$ with kinetic energies from 10 MeV to 200 MeV . The traces exhibit a distinct maximum in particle numbers and a bandwidth limited energy distribution for charge states $Z > 25$. The low energetic cutoff for ions charged $Z < 25$ probably lies beyond the detection range. The symmetry of the gold ions cutoff on the detector seems to follow a lemniscate like function (half figure eight): $r(\phi(Z)) \sim a^2 \times 2 \sin(2\phi(Z))$, with a as a constant of the radius and $\phi(Z)$ a nonlinear, charge depending function. We evaluated the highest energy cutoff and lowest energy cutoff for the different charge states of gold ions in Fig.2. Compared to an expected $E_{kin}^{Max} \propto Z^2$ scaling by the model of [13], our data shows a boosted scaling of $E_{kin}^{Max} \propto (Z-6)^{2.7}$. For a better comparison Fig.2 uses the same scaling coefficient for both fit functions. Experiments with gold coated plastic foils (Formvar $(10-40) \text{ nm}$ + $(2-6) \text{ nm}$ gold coating on target rear side) showed similar results concerning the multiple degrees of ionization, the Z to E_{kin}^{Max} scaling, reaching close to the MeV/u range and with a limited bandwidth in the energy spectrum (see supplement [35]). It reveals a general mechanism for the acceleration of heavy ions

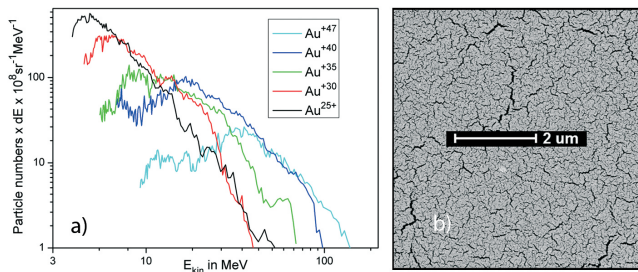


FIG. 3: **a**: The associated evaluated energy distribution for selected, single traces of gold ions of Fig.1 and Fig.2 is shown, exhibiting a pronounced maximum. dE is given by the binning of the spectrometers resolution. **b**: STEM measurement of freestanding target foil reveals a crack like structure. Dark cracks mark here the carbon substrate layer.

ultra thin foil with heavy material is used. The energy distribution related to Fig.1 of selected gold ions is shown in Fig.3. The particle numbers are given relative to a detector calibration with hydrogen and carbon, assuming a similar response for heavy ions [36]. The divergence of the heavy ion beam is assumed with 3° , as it is smaller compared to the protons one [37]. Here we inferred theoretically from a divergence measurement of the protons (for methods see supplement [35, 38]) by using the same acceleration field. Our latest theoretical findings indicate a dependency on charge and mass number [35]. We approximate the energy content of all accelerated gold ions with to 5% of the laser energy, while the H^+ reaches < 2%.

In order to account for the theoretical ionization Z in dependence on the electrical field strength a_0 we used the ADK model [39] as collision ionization is not significant for our case. The calculation for gold is shown in Fig.3a) and we find an ionization dependence $Z(a_0) = 23 \times a_0^{0.4}$. The field strength for our parameters considers an intensity of $a_0 = 5$, which leads to a maximum ionization of $Z(a_0) = 42$. Higher ionization as observed in our experiment can be attributed to field enhancement in case of partly transparent target plasma, to contributions from the surface structure and to self focusing.

Our 1D PIC simulation considered a dynamic ionization and was evaluated at high accuracy (mesh size: 0.16 nm, 200 particles per cell, error < 1%) has been performed using the laser parameters of the experiment and a target thickness of 20 nm. For simplification we froze the ionization in time at the end of the laser pulse. The 1D PIC simulation shows in longitudinal direction a symmetrical, varying ionization degree $Z(z)$ (see Fig.4b) [40]. Compared to an averaged degree of ionization, it leads to an enhancement of the electrical field at the front and rear side of the target by contributions of the repelling Coulomb force. The field enhancement becomes strong for highly charged ions. For the 2D PIC simulation we used the ionization distribution of the 1D PIC simulation,

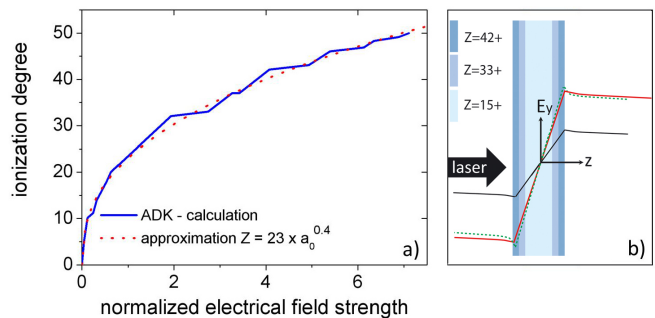


FIG. 4: **a**: The dependence of gold ionization on the electric field E_L in units of a_0 calculated with the ADK Model. The dashed line (red) fits $Z(a_0) = 23 \times a_0^{0.4}$. **b**: E_L calculated from analytical model (red) and PIC simulation (green) considering ion layers of the following degrees of ionization: The distribution of ion charge is: 0 – 1nm $Z = 42$, 1 – 2nm $Z = 33$, 2 – 18nm $Z = 15$, 18 – 19nm $Z = 33$, 19 – 20nm $Z = 42$. Black line - E_L calculated with an averaged ionization degree of $Z = 15$.

at 5×10^{19} W/cm², 35 fs, 4 μ m focus diameter, Gaussian laser profile. The pulse interacts with a pure 20 nm thick gold target. The step size of the calculation was 0.5 nm with 30 particles per cell. In Fig.5 we compare the calculated energies with our experimental results and the model of [13]. The E_{kin}^{Max} to Z dependence has to be separated into three parts: while for $Z < 15$ the Au ion energies fit to a $E_{kin}^{Max} \sim Z^2$, ions with $Z > 15$ are with an exponent > 2 , followed by a smaller linear dependence for $Z > 42$.

Our analytical model focuses on the Poisson equation, as the electrical field of the laser does not penetrate deep inside even in our thin foil. We take a spatially varying ionization of heavy target material into account:

$$2\left(\frac{\partial^2 \eta_e}{\partial \xi^2} + \frac{\partial^2 \eta_e}{\partial \varsigma^2}\right) = \eta_e - Z(E)n_{i0}\Theta\left(\frac{l_f}{2} - |\xi|\right)\Theta\left(\frac{l_e}{2} - |\varsigma|\right) \quad (1)$$

Here we use a 2D geometry with the coordinates $(z, y) = (\xi, \varsigma)r_D$, where the Debye radius is $r_D^2 = T_H/4\pi e^2 n_{eH}$ and assuming the process to be adiabatic. The normalized electron density is $\eta_e = n_e/n_{eH} = 1 + \phi/2$ and the normalized electric field is $E = \frac{2c}{\omega r_D} \frac{\partial \eta_e}{\partial \xi}$. The ion density $n_i(z, y) = \eta_{i0}\Theta(z)\Theta(y)n_{eH}$ has a rectangular shape in both directions, where $L_{f,e}(t) = l_{f,e}(t)r_D$ are dynamic foil thickness and electron spot size, respectively. The hot electron density is determined from quasi-neutrality and the ionization degree is $Z(E) = 23E^{0.4}$. We introduce a spatial dependence of the hot electron density: $n_{eH} \approx \frac{\pi e^2 n_i^2}{T_H} \left(\int_0^{l_f} Z(\xi)\right)^2$. The spatial dependence of ionization is given as:

$$Z(\xi) = 23 \times \left(\frac{2c}{\omega r_D} \frac{\partial \eta_e}{\partial \xi}\right)^{0.4} \quad (2)$$

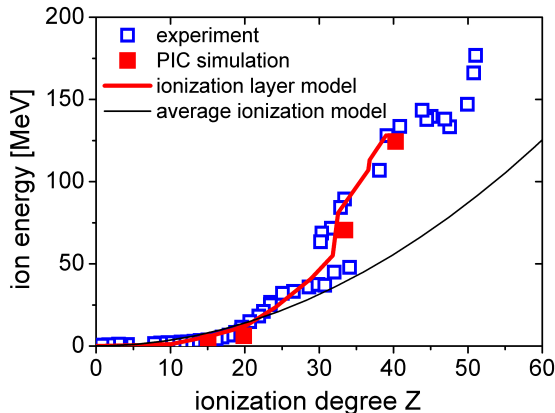


FIG. 5: The dependence of maximal ion energy on its ionization degree: the experimental data of Fig.2 - deep blue squares, 2D PIC - simulation data - red squares, Schreiber model - black line and our model - red line. The distribution of ion ionization is according to the 1D PIC simulation in Fig.4.

The electron temperature T_H depends on the pulse duration τ_L and on a laser absorption coefficient κ (here and in the following see [41]): $T_H(l_f) \approx \frac{\kappa(l_{f0})I_L\tau_L}{n_{eh}l_{f0}}$. For simplification, we assume a rectangular transversal (y) and longitudinal (z) electron density profile, which width changes in time with $l_f(t)$. For the ultrathin foil follows: $\Theta(l_f(t)/2 - |\xi|) \rightarrow l_f(t)\delta(\xi)$, we take the expansion of the recirculating hot electrons as a time dependent parameter $l_e(t)$. At this point we freeze the degree of ionization in time. The time dependent solution of Eq.1 at $|z| \geq l_f(t)/2$ looks similar to [41]:

$$E(z, y, t) = 4\pi en_{i0} \frac{\text{sign}(z)\Theta(l_e(t) - |z|)}{1 + \sigma_c t r_D l_f(t)/D_0^2} \times \int_0^{l_{f0}} Z(\xi) d\xi \exp(-|\xi| + \frac{l_{f0}}{2}) \quad (3)$$

D_0 denotes the initial electron spot size and σ_c is the plasma conductivity. The equation contains a spatial dependence of the charge distribution in the target instead of an averaged, constant one. The dependence of the analytical field (3) on coordinate z is similar to the PIC simulated one (Fig.4b). The charged ion front $l_f(t)$ in the target can be calculated by the equation of motion after inserting (3) and with $C = 16\pi e^2 l_{f0} n_{i0}/m_i$:

$$l_f(t) = l_{f0} + t \sqrt{C \times Z(l_{f0}) \left[\int_0^{l_{f0}} Z(\xi) d\xi \right] \ln\left(\frac{l_f(t)}{l_{f0}}\right)} \quad (4)$$

Expression (4) defines the energy of an ion with maximum degree of ionization, which is at the front of acceleration $\varepsilon_{Z(l_{f0})} = m_i \dot{l}_f^2(t)/8$. Electron density in each

instant is defined by (1). From the equation of continuity follows $n_i(z, t) = n_i l_{f0} \Theta(l_f/2 - |z|)/l_f(t)$ and the ion velocity with the coordinate of z reads: $v_i(z, t) = z \dot{l}_f(t)/l_f(t)$, $|z| < l_f(t)/2$. The energy for a particle placed initially at ξ_0 with an charge of $Z(\xi_0)$ has to be evaluated parametrically with (2) and (4). For ions inside the target $\xi_0 \in [0, l_f/2]$ results:

$$\varepsilon_z(\xi, t^*) = \frac{m_i}{2} (\xi_0/l_{f0})^2 \dot{L}_f^2(t^*) \quad (5)$$

With $t^* \approx D_0^2/\sigma_c r_D l_f$ for ions of very high energy $t^* \sim 2\tau_L$ [12]. This leads to $\sim Z^3$ ion energy to charge scaling, which is in good agreement with our PIC simulated and experimental results (see Fig.5). Ions with a very high degree of ionization $Z > Z(l_{f0})$, are formed in a field maximum at the target rear side. These ions have the initial coordinate $\xi_0 = l_{f0}$. According to (4) $\dot{l} \approx \sqrt{Z(l_{f0})}$ for ions with a high charge Z , the formula (5) gives for all $Z > 42$ the linear relation $\varepsilon_Z \sim Z$. The smaller energy to Z scaling is explained by the decreasing charged background compared to ions placed inside the target.

In conclusion, we demonstrated efficient acceleration of heavy ions by an ultra short laser pulse system. So far laser systems that compensate lower laser energy with a shorter pulse duration to reach the same intensity, had not been able to accelerate heavy ions with $A > 12$ into the MeV/u region. By using an ultra thin foil of heavy material we achieved highly charged heavy ions with a limited bandwidth in the energy spectrum, reaching up to 1 MeV/u. Furthermore we simplified a complex target preparation, which achieves a prerequisite for future applications. We demonstrated experimentally and theoretically how a spatial distribution of the ionization inside the target leads to a field enhancement for the heavy ions by Coulomb explosion. This has the potential to greatly improve the efficiency of heavy ion acceleration by stronger kinetic energy with charge scaling. Our results indicate that e.g. energies with 7 MeV/u can be achieved with ~ 50 times higher laser energy than in our experiment. This relaxes the previously estimated laser power requirements for upcoming facilities [7] by a factor of 3 which is enormous in costs if ultra fast $\sim 100J$ class lasers are considered.

The research leading to these results received funding from the Deutsche Forschungsgemeinschaft within the program CRC/Transregio 18 and LASERLAB-EUROPE (grant agreement n 284464, EC's Seventh Framework Program). Computational resources was provided from the ISC within the project MBU15.

[1] T. E. Cowan, J. Fuchs, H. Ruhl, A. Kemp, P. Audebert, M. Roth, R. Stephens, I. Barton, A. Blazevic, E. Brambrink, et al., Physical Review Letters **92**, 204801 (2004).

- [2] V. Scuderi, S. Bijan Jia, M. Carpinelli, G. A. P. Cirrone, G. Cuttone, G. Korn, T. Licciardello, M. Maggione, D. Margarone, P. Pisciotta, et al., *Nuclear Instruments and Methods in Physics Research Section A* **740**, 87 (2014).
- [3] D. Schardt, T. Elsässer, and D. Schulz-Ertner, *Reviews of Modern Physics* **82**, 383 (2010).
- [4] T. Tajima, D. Habs, and X. Q. Yan, *Rev. Acc. Science Technol.* **2**, 201 (2009).
- [5] C. Hill, *Cern linac 2*, URL <http://www.cern.ch/linac2/web.cern.ch/linac2/>.
- [6] M. Hegelich, S. Karsch, G. Pretzler, D. Habs, K. Witte, W. Guenther, M. Allen, A. Blazevic, J. Fuchs, J. C. Gauthier, et al., *Physical Review Letters* **89**, 085002 (2002).
- [7] G. Morou, G. Korn, W. Sandner, and J.L. Collier, *The whitebook of ELI Nuclear Physics group* (Thoss-Media GmbH, 2011).
- [8] H. Daido, M. Nishiuchi, and A. Pirozhkov, *Rep Prog Phys* **75**, 056401 (2012).
- [9] G. Kraft, *Tumor Therapy with Heavy Ions* (Verein zur Förderung der Tumorthherapie mit schweren Ionen e.V., 2007).
- [10] B. M. Hegelich, B. J. Albright, J. Cobble, K. Flippo, S. Letzring, M. Paffett, H. Ruhl, J. Schreiber, R. K. Schulze, and J. C. Fernandez, *Nature* **439**, 441 (2006).
- [11] B. M. Hegelich, B. Albright, P. Audebert, A. Blazevic, E. Brambrink, J. Cobble, T. Cowan, J. Fuchs, J. C. Gauthier, C. Gautier, et al., *Physics of Plasmas* **12** (2005).
- [12] P. Mora, *Physical Review E* **72**, 056401 (2005).
- [13] J. Schreiber, F. Bell, F. Grüner, U. Schramm, M. Geissler, M. Schnürer, S. Ter-Avetisyan, B. M. Hegelich, J. Cobble, E. Brambrink, et al., *Physical Review Letters* **97**, 045005 (2006).
- [14] J. Schreiber, *Ion acceleration driven by high-intensity laser pulses* (2006), URL http://edoc.ub.uni-muenchen.de/5842/1/Schreiber_Joerg.pdf.
- [15] S. C. Wilks, A. B. Langdon, T. E. Cowan, M. Roth, M. Singh, S. Hatchett, M. H. Key, D. Pennington, A. MacKinnon, and R. A. Snavely, *Physics of Plasmas* **8**, 542 (2001).
- [16] T. Esirkepov, M. Yamagiwa, and T. Tajima, *Physical Review Letters* **96**, 105001 (2006).
- [17] B. Qiao, M. Zepf, M. Borghesi, B. Dromey, M. Geissler, A. Karmakar, and P. Gibbon, *Physical Review Letters* **105**, 155002 (2010).
- [18] A. Henig, S. Steinke, M. Schnürer, T. Sokollik, R. Hörlein, D. Kiefer, D. Jung, J. Schreiber, B. M. Hegelich, X. Q. Yan, et al., *Physical Review Letters* **103**, 245003 (2009).
- [19] X. Q. Yan, C. Lin, Z. M. Sheng, Z. Y. Guo, B. C. Liu, Y. R. Lu, J. X. Fang, and J. E. Chen, *Physical Review Letters* **100**, 135003 (2008).
- [20] D. Jung, L. Yin, D. C. Gautier, H. C. Wu, S. Letzring, B. Dromey, R. Shah, S. Palaniyappan, T. Shimada, R. P. Johnson, et al., *Physics of Plasmas* **20**, 083103 (2013).
- [21] X. Q. Yan, T. Tajima, M. Hegelich, L. Yin, and D. Habs, *Applied Physics B* **98**, 711 (2010).
- [22] S. Steinke, A. Henig, M. Schnürer, T. Sokollik, P. V. Nickles, D. Jung, D. Kiefer, R. Hörlein, J. Schreiber, T. Tajima, et al., *Laser and Particle Beams* **28**, 215 (2010).
- [23] S. Steinke, P. Hilz, M. Schnürer, G. Priebe, J. Braenzel, F. Abicht, D. Kiefer, C. Kreuzer, T. Ostermayr, J. Schreiber, et al., *Physical Review Special Topics - Accelerators and Beams* **16**, 011303 (2013).
- [24] T. Z. Esirkepov, S. V. Bulanov, K. Nishihara, T. Tajima, F. Pegoraro, V. S. Khoroshkov, K. Mima, H. Daido, Y. Kato, Y. Kitagawa, et al., *Physical Review Letters* **89**, 175003 (2002).
- [25] B. Qiao, S. Kar, M. Geissler, P. Gibbon, M. Zepf, and M. Borghesi, *Physical Review Letters* **108**, 115002 (2012).
- [26] S. S. Bulanov, A. Brantov, V. Y. Bychenkov, V. Chvykov, G. Kalinchenko, T. Matsuoka, P. Rousseau, S. Reed, V. Yanovsky, D. W. Litzenberg, et al., *Physical Review E* **78**, 026412 (2008).
- [27] H. Y. Wang, C. Lin, B. Liu, Z. M. Sheng, H. Y. Lu, W. J. Ma, J. H. Bin, J. Schreiber, X. T. He, J. E. Chen, et al., *Physical Review E* **89**, 013107 (2014).
- [28] A. V. Korzhimanov, E. S. Efimenko, S. V. Golubev, and A. V. Kim, *Physical Review Letters* **109**, 245008 (2012).
- [29] M. Kalashnikov, K. Osvay, R. Volkov, H. Schönengel, and W. Sandner, *CLEO 2011 - Laser Applications to Photonic Applications* p. CWG3 (2011).
- [30] A. Levy, T. Ceccotti, P. D'Oliveira, F. Reau, M. Perdrix, F. Quere, P. Monot, M. Bougeard, H. Lagadec, P. Martin, et al., *Optics Letters* **32**, 310 (2007).
- [31] J. Braenzel, C. Pratsch, P. Hilz, C. Kreuzer, M. Schnürer, H. Stiel, and W. Sandner, *Review of Scientific Instruments* **84**, 056109 (2013).
- [32] A. A. Andreev and K. Y. Platonov, *Contributions to Plasma Physics* **53**, 173 (2013).
- [33] T. Ceccotti, V. Floquet, A. Sgattoni, A. Bigongiari, O. Klimo, M. Raynaud, C. Riconda, A. Heron, F. Baffigi, L. Labate, et al., *Physical Review Letters* **111**, 185001 (2013).
- [34] T. Sokollik, *Investigations of Field Dynamics in Laser Plasmas with Proton Imaging*, Springer Theses (Springer Berlin Heidelberg, 2011).
- [35] J. Braenzel, *Supplemental material*, URL <http://www.http://prl. ./>.
- [36] R. Prasad, D. Doria, S. Ter-Avetisyan, P. Foster, K. Quinn, L. Romagnani, C. Brenner, J. Green, P. Gallegos, M. Streeter, et al., *Nuclear Instruments and Methods in Physics Research Section A* **623**, 712 (2010).
- [37] E. Brambrink, J. Schreiber, T. Schlegel, P. Audebert, J. Cobble, J. Fuchs, M. Hegelich, and M. Roth, *Physical Review Letters* **96**, 154801 (2006).
- [38] F. Nürnberg, M. Schollmeier, E. Brambrink, A. Blažević, D. C. Carroll, K. Flippo, D. C. Gautier, M. Geiel, K. Harres, B. M. Hegelich, et al., *Review Scientific Instruments* **80**, 033301 (2009).
- [39] M. Ammosov, A. Delone, and V. Krainov, *Sov. Phys. JETP* **64**, 1191 (1986).
- [40] A. Zhidkov and A. Sasaki, *Physics of Plasmas* **7**, 1341 (2000).
- [41] A. A. Andreev, S. Steinke, M. Schnuerer, A. Henig, P. V. Nickles, K. Y. Platonov, T. Sokollik, and W. Sandner, *Physics of Plasmas* **17**, 123111 (2010).